Composites Part B 191 (2020) 107965

Contents lists available at ScienceDirect

Composites Part B

journal homepage: www.elsevier.com/locate/compositesb

Wide and fine alignment control and interface modification for high-performance thermally conductive graphite/copper composite

Huaijie Cao, Zhanqiu Tan **, Genlian Fan, Qiang Guo, Yishi Su, Zhiqiang Li, Ding-Bang Xiong *

State Key Laboratory of Metal Matrix Composites, Shanghai Jiao Tong University, Shanghai, 200240, China

ARTICLE INFO

Dedicated to Professor Bernd Harbrecht on the occasion of his 70th birthday.

Keywords:
Thermal conductivity
Graphite
Graphene
Copper

ABSTRACT

A controlled alignment of micro-/nano-fillers with anisotropic morphology and properties in a composite matrix will allow developing materials with tailored properties, but which still remains challenging. Here, alignment of graphite plates in Cu matrix was well controlled in a wide range with fine steps by elaborately designed morphologies of copper powders. Polarized Raman scattering demonstrated that a record-high orientation degree could be obtained as assisted by Cu micro-flakes. Furthermore, owing to the improvements on intrinsic thermal conductivity of graphite by hot-pressing and graphite/Cu interface wettability by using in-situ graphene as interlayer, high-performance thermally conductive (~600 W/mK) and light-weight (4.9 g/cm^3) graphite/graphene-interlayer/Cu matrix composites were successfully fabricated.

1. Introduction

Operation of microelectronic devices generates heat in a confined space making heat dissipation a key challenge [1–3]. Carbon (diamond, carbon nanotube, graphene, graphite)/copper composites are considered as promising materials in thermal management for microelectronic devices with higher and higher power density. However, diamond suffers from high cost, slow synthesis rates and poor machinability, while the thermal conductivity (TC) of carbon nanotube (CNT) and graphene (Gr) degrade when assembled into practical size due to ambient interactions and disorder scattering [3], which limits their wide application. Graphite flakes (Gf) have drawn significant attention for thermal management applications due to their superior and stable thermal properties, low cost and ease of machining [4–7].

The carbon materials (carbon nanotubes, graphene, graphite flakes) show anisotropic TC along different dimensions [8,9]. In the composites, a high alignment of the carbon structures is necessary for improving the TC [10–14]. It has been reported that Gf exhibits an in plane TC higher than 1000 W/mK [6]. Highly oriented pyrolytic graphite (HOPG) has a TC of 1600–2000 W/mK [15,16]. Whatever the graphite type, an out-of-plane TC of 5–10 W/mK has been reported [15]. A critical value of the alignment of graphite in matrix [12] exists, above which the contribution of high in-plane TC of graphite will surpass the negative role of its low out-of-plane. It is very challenging to align nanoscaled CNT or Gr in composites [10,12,17–19], and also it is by no means easy to achieve high alignment of graphite in a composite although it has larger size than CNT and Gr [20,21]. In graphite/Cu (Gf/Cu) composites, several methods, such as electroless plating [22,23], wet mixing [24] and high-energy ball milling [13,20], were applied to align graphite within Cu matrix. Liu et al. [22] used electroless plating to prepare 71 vol% Gf/Cu composite with a TC of 565 W/mK. The orientation degree ($<\cos^2\theta>$) [12,13,18,20] of graphite in the composite was estimated to be 0.8 from effective medium approximation (EMA) model. Electroless plating method is usually limited for preparing small and thin samples due to the slow deposition rate of Cu layers. A orientation degree ($<\cos^2\theta>$) of 0.81 and a TC of 547 W/mK were obtained in 60 vol% Gf/Cu composite prepared by a wet mixing method [24]. This method is time-consuming and induces degradation of graphite by chemical contamination, plastic deformation or by local overheating [25]. Boden et al. reported that the alignment of graphite in copper matrix could be controlled by optimizing the lateral size of graphite flakes [20], and the value of $<\cos^2\theta>$ ranged from 0.54 to 0.69 in the final Gf/Cu composites [20]. Nevertheless, the TCs of the as-produced <30 vol% Gf/Cu composite were lower than that of the pure Cu matrix, because the orientation degree ($<\cos^2\theta> = 0.69$) of the graphite was still below the critical value. Subsequently, they prepared a 50 vol% Gf/Cu composite by the same method and obtained a higher orientation degree ($<\cos^2\theta> = 0.8$) of graphite, resulting in an enhanced TC of 503 W/mK [13]. Thus,

* Corresponding author.
** Corresponding author.
E-mail addresses: tanzhanqiu@sjtu.edu.cn (Z. Tan), xiongdingbang@sjtu.edu.cn (D.-B. Xiong).

https://doi.org/10.1016/j.compositesb.2020.107965
Received 2 November 2019; Received in revised form 6 March 2020; Accepted 7 March 2020
1359-8368/© 2020 Elsevier Ltd. All rights reserved.

developing an effective strategy for realizing orientation degree of graphite as high as possible is desired for enhancing the TC in Gf/Cu composite.

Additionally, graphite/Cu composites still possess poor interface bonding and voids because of poor wettability between graphite and Cu matrix [26,27], which are usually improved by two common approaches, *i.e.*, surface metallization (B, Cr, Zr, Cu, W, Ti, Si, Mo) [6,22,28–33] on graphite and matrix alloying (Cr, Ti) [34,35]. While these methods still face the following challenges, (1) selecting desirable carbide formed elements or interlayer [36]; (2) tailoring thickness and morphology of the interlayer [37]; (3) controlling complete interface reaction process (formation of carbides) in composite [38]. Graphene, with intrinsic 2D structure as well as high in plane TC [39], could act as interlayer to enhance the TC of carbon/Cu composites, by bridging the phonon transport and avoiding direct contact between Cu and graphite [40]. The advantages of graphene as interlayer lie in (1) thickness of the uniform nanolayer of the graphene is tunable; (2) compared to the aforementioned carbide or metal elements, graphene exhibits a lower density and a higher TC; (3) interface is free of reaction product.

In this work, the strategies for controlling alignment of graphite flakes in Cu matrix and interface modification are successfully developed, and light-weight Gf/Cu composites with enhanced TC and satisfied coefficient of thermal expansion (CTE) are thus fabricated. The relationship between alignment degree of graphite flakes and thermal conductivity is quantitatively analyzed with polarized Raman spectroscopy. We show that the alignment is inseparably linked to the morphology and thickness of the elaborately designed flaky Cu powder (FCu). This relationship results in anisotropic thermal properties of the composites (up to a factor of 8.5). An EMA model is used for accounting the experimental results, in which the influence of filler geometry, orientation degree as well as the interfacial thermal resistance between matrix and filler are considered.

2. Experimental

2.1. Materials

Spherical copper powders (particle size: ~50 μm, ~2–3 μm) polymethyl methacrylate (PMMA) (M.W. 35000) and graphite flakes (purity >99.9%, mesh −10) were purchased from Alfa Aesar Chemical Co., Ltd, Tianjin, China. Absolute ethanol and anisole were obtained from Sinopharm Chemical Reagent Co., Ltd, Shanghai, China. The chemicals were analytical-grade reagents and were used as received.

2.2. Fabrication of composites

Spherical copper powders (100 g) with an averaged particle size of 50 μm were ball milled in a stainless-steel milling jar at a speed of 423 rpm for different time (4, 6 or 14 h) in absolute ethanol. The mass ratio between Cu powder (100 g) and agate milling ball (800 g) is about 1:8. The in-situ growth of graphene on Cu powders was reported in our previous work [40,41]. Prior to in-situ growth process, the as-prepared flaky powders were annealed and reduced at 5% H_2/Ar mixed atmosphere at 573 K. And then 30 g annealed flaky Cu powders (FCu) were added into 250 mL 0.5 wt% PMMA-anisole solution. The mixture was stirred for 12 h, and then centrifuged at 4000 rpm for 7 min. After that, the PMMA coated flaky Cu powders were dried in a vacuum oven at 343 K for 12 h to remove the solvent. The in-situ growth process was performed in a tube furnace under H_2 (25 sccm) and Ar (475 sccm) flow at atmospheric pressure. The dried PMMA/FCu powders were placed in an alumina crucible and were heated rapidly to 1173 K at a heating rate of 10 K/min. The temperature was kept for 1 h. Finally, graphene/FCu (Gr/FCu) composite powders were obtained by fast-cooling to room temperature under the H_2/Ar atmosphere. The pristine graphite flakes were sieved through a 40-mesh screen prior to use. The as prepared Gr/FCu powder and graphite flakes were mixed and then densely stacked when loaded into a graphite die (Ø 20 mm). The powders were heated up to 1173 K in vacuum at a heating rate of 15 K/min and sintered at the temperature under a pressure of 50 MPa for 1 h. For comparison, the Cu, Gr/Cu, Gf/SCu and Gf/FCu samples without graphene were prepared by the same method. The whole preparation process is shown in Fig. 1.

2.3. Characterization on microstructure and composition

The microstructures of the composited powders and bulk composites were examined by using scanning electron microscope (SEM, Mira3) and transmission microscope (TEM) (JEOL JEM-2100F). Raman spectra (Bruker Optics Senterra R200-L) were used to characterize the graphite and graphene by using Ar + laser with a wavelength of 532 nm (spot size 1 μm and laser power 1 mW) as excitation source. Energy-dispersive X-ray spectroscopy (EDS) was used for elemental analysis. X-Ray diffraction (XRD) test was performed on a Rigaku D/max2550VL/PC system with Cu Kα radiation generated at 35 KeV and 200 mA ($\lambda = 0.15418$ nm). The 2θ step size was 0.02°. X-ray computed tomography (diondo d2, GE Company) was used for visualizing the distribution of graphite flakes in the Gf/Cu composites.

2.4. Graphite alignment measurement

The rough and fractured cross-section of Gf/Cu matrix composite was mechanical polishing and then milled by surface ion-beam (Ar + polisher) before Raman spectra measurements. Polarized Raman spectroscopy was carried out on the cross-section of Gf/Cu matrix composite (excitation wavelength 532 nm and power 1 mW). Grating was 1800 l/mm and integration time was 1 s. The light was focused by a 5 × objective; the spectra were recorded on a Renishaw Centrus 0RNQ39 monochromator. The polarizations of the incoming and scattered light were parallel to each other. The angle between the polarization direction and the sample normal was rotated with a λ/2 wave plate in front of the microscope objective.

2.5. Thermal conductivity and coefficient of thermal expansion measurements

The TC of the composites was calculated according to $\kappa = \alpha \times \rho \times C_p$. Thermal diffusivity (α) and specific capacity (C_p) of the sintered composites were measured by a laser flash method on a Netzsch LFA 427 at room temperature (298 K). The sample density (ρ) was examined by the Archimedes method. The samples (Ø 12.6 × 3 mm) were coated with carbon using a carbon spray on the top and bottom surfaces to prevent the laser light and plasma generation at the surface. Five parallel positions were measured to obtain an average TC value for each sample. The samples with a dimension of Ø5 × 25 mm were cut for coefficient of thermal expansion (CTE) measurement, and the CTE of both in-plane and cross-plane directions were measured on dilatometer (NETZSCH DIL 402 C) in a temperature range of 300–575 K with a heating rate of 3 K/min.

3. Results and discussion

3.1. Microstructure and thermal conductivity of graphite flakes

Fig. 2a–b shows the SEM images of the typical morphology for the sieved graphite flakes. The lateral size of the graphite flakes varies from 450 to 550 μm with an average thickness of 20 μm. TEM image, XRD pattern and Raman spectra in Fig. S1 (Supporting Information) confirm the structure and composition of the as received graphite.

According to Adams' conclusion [42], in-plane TC of graphite shows an inseparable relation with its inter-basal-plane spacing $d_{(002)}$, i.e., the smaller $d_{(002)}$ is, the higher TC of graphite. Furthermore, removing defects (vacancies, interstitials and impurities) could lead to an increased

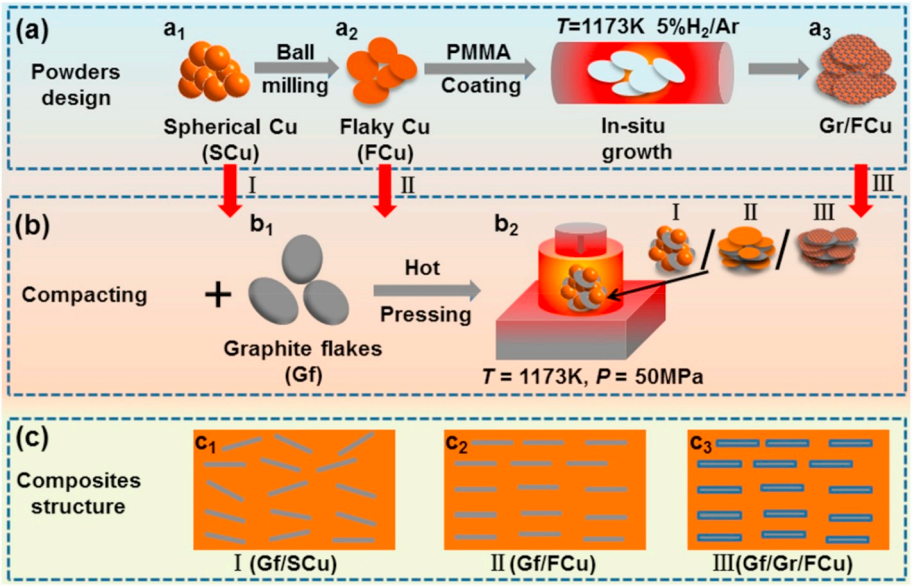

Fig. 1. Schematic illustration of preparation process of Gf/SCu, Gf/FCu and Gf/Gr/FCu (Gr: graphene) composites: (a) fabrication of flaky Cu powder (FCu) and graphene encapsulated Cu powder (Gr/FCu); (b) compacting powders by a hot-pressing process, and (c) the structural models for the as-prepared composites.

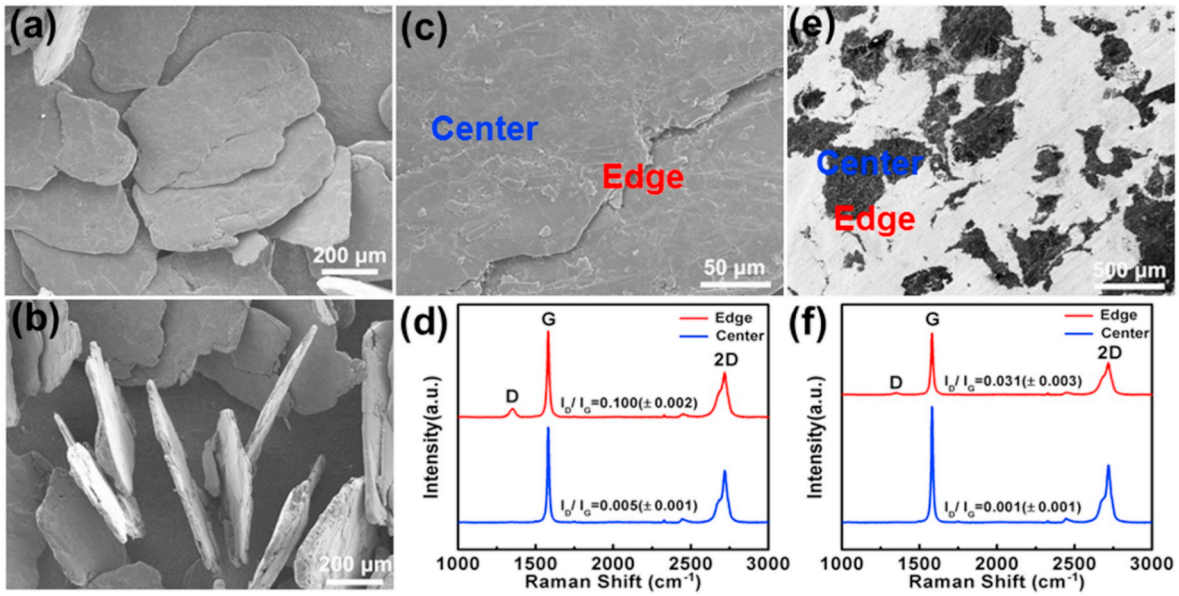

Fig. 2. SEM images of graphite flakes to show lateral size (a) and thickness (b); (c–f) the micrograph and Raman spectra at both centre and edge of as received graphite flake (c–d) and graphite flake (e–f) in the composite after hot pressing.

layer plane stacking. Here, our XRD patterns show that the hot-pressing process can cause an apparent change on the $d_{(002)}$ of graphite, and the peak position of plane (002) decreased from $2\theta = 26.38°$ in the as-received graphite (Fig. S1c, Supporting Information) to a value of $2\theta = 26.5°$ in the graphite embedded in the hot-pressed Gf/FCu composites (Figs. S2 and S3, Supporting Information). According to the Bragg equation, the $d_{(002)}$ of graphite flakes decreases from 3.378 Å (as-received) to 3.363 Å after the hot-pressing process. Based on the correlation between the TC and $d_{(002)}$ established by Adams [42], the estimated in-plane TC of the graphite flake in the hot-pressed composite after is close to 1020 W/mK, while that of as-received graphite flake is only ~500 W/mK. The results is also coherent with the Raman spectra of graphite flakes before and after hot-pressing (Fig. 2d,f). The spectra at both the centre and edge (Fig. 2c,e) of the graphite flakes imply that the hot-pressing process helps to decrease the I_D/I_G ratio (i.e. increase graphite's quality and thus its TC), which is more obvious on the edges of the flakes.

Morvan et al. [25] proposed a reductive treatment of graphite flakes at 400 °C to obtain a low $d_{(002)}$ value of 3.360 Å, indicating a high TC of with 1100 W/mK. Other method, such as chemical pre-treatment [23], was adopted to remove the surface adhesive contamination of graphite for improving the TC. In previous studies, TC of graphite in the composite is usually estimated as 1000 W/mK from pyrolytic graphite for EMA calculation and it has seldom considered the influence of hot-pressing process on the TC of composite. In this study, the hot-pressing process at high temperature (1173 K) and high pressure (50 MPa) can improve the TC of graphite, which may result from the improved crystallinity structure of graphite and removal of defects compared to the as received graphite. Our results indicate that the change in TC of graphite before and after hot-pressing process should be

considered because it directly affects the theoretical value from EMA.

3.2. Morphology effect of Cu powder on graphite's alignment

To regulate the alignment of graphite flakes in matrix, the morphology and size effect of Cu matrix powder is investigated in this work. Firstly, spherical Cu powders with diameter ~50 μm and 2–3 μm were used as matrix. The pristine morphologies of the Cu powders and graphite distributed in composites are shown in Fig. 3. In the case of spherical Cu as matrix, the large size (~50 μm) leads to a random orientation of graphite flakes in the composites (Fig. 3a–b). As shown in Fig. 3c–d, the orientation of graphite is improved when smaller spherical Cu powders (2–3 μm) were used as matrix, but the graphite flakes accumulate in some area and show a poor distribution in the composite. The results imply that the spherical morphology might not be the ideal choice for aligning graphite flakes in Cu matrix.

Considering the morphology compatibility, Cu powder with flaky shape were therefore used to regulate the orientation of graphite flake in the composites; Meanwhile, the thickness effect of Cu flakes on the alignment of graphite were also investigated. For comparison, Cu flakes with an averaged thickness of 20–30 μm, 10–20 μm and 1–2 μm were used. As shown in Fig. 4, the flaky morphology of Cu powder can realize a high orientation of graphite. Moreover, the thicker Cu flakes (20–30 μm, 10–20 μm) result in a smaller spacing between two graphite flakes (marked in Fig. 4b,d) than that the thinner Cu flakes (1–2 μm) do (marked in Fig. 4e). Given the same content of graphite, the larger spacing indicates the better alignment of graphite in the composite because of a smaller projected cross section. Thus, the flaky Cu powders make it effective to align graphite in the composite compared with spherical powders (Fig. 3). During the mixing process and compaction process, flaky Cu powders with larger specific surface area and better morphology compatibility with graphite flakes contribute to uniform dispersion and high alignment of graphite in the composite.

Three-dimensional X-ray computed tomography (3D X-CT) was adopted to visualize distribution of graphite flakes in the Gf/Cu composite. As shown in both 3D (Fig. 5a–b) and 2D (Fig. 5c–d) images, graphite flakes with similar sizes are distributed in the composites. The disordered distribution of graphite flakes is observed in Gf/SCu composite with spherical Cu as matrix (Fig. 5a,c), while graphite flakes are highly aligned in the whole Gf/FCu composite with flaky Cu as matrix (Fig. 5b,d), which agrees well with the SEM images (Figs. 3a and 4f). The results suggest that flaky matrix power with as thin as possible thickness is beneficial for the alignment of graphite flakes.

3.3. Quantitative analysis on alignment

Polarized Raman spectra was used for quantitating the alignment of graphite flakes in the composites. Fig. 6a shows the schematic illustration of measurement setup. In Fig. 6b, theoretically, for a random distribution of the graphite (red curve), intensity of the *G*-peak is a constant when varying the polarization angle ε. For perfectly aligned graphite (blue curve), the intensity of *G*-peak $I_{tot} \propto f\ ^2\cos^4\varepsilon$ and thus has a maximum for the in-plane polarization ($\varepsilon = 0$, 180°, and 360°), while it is zero for $\varepsilon = 90°$, 270° [13,20]. Fig. 6c–d shows the normalized intensity of the G-mode measured for the Gf/Cu composites with different Cu matrix as matrix. Comparing the intensity of G band ratio (I_{min}/I_{max}) of composites, the statistical orientation shows that graphite flakes embedded in flaky Cu (~1–2 μm) have the best alignment compared with the those in the other Cu powders as matrix.

Orientation degree of the graphite flakes can be evaluated by the parameter of $<\cos^2\theta>$, which is determined by the θ value, and is expressed as [43]

$$\langle \cos^2\theta \rangle = \frac{\int \phi(\theta)\cos^2\theta \sin\theta d\theta}{\int \phi(\theta)\sin\theta d\theta} \quad (1)$$

where θ is the angle (0–90°) between graphite flakes basin plane and the perpendicular direction of the hot pressing. $\phi(\theta)$ describes the statistical distribution of graphite orientation in the composites, which can be determined by the results of polarized Raman spectra. Theoretically, $<\cos^2\theta> = 1/3$ and 1 stand for totally random orientation and perfectly full alignment of graphite flakes in the composite (Fig. S4, Supporting

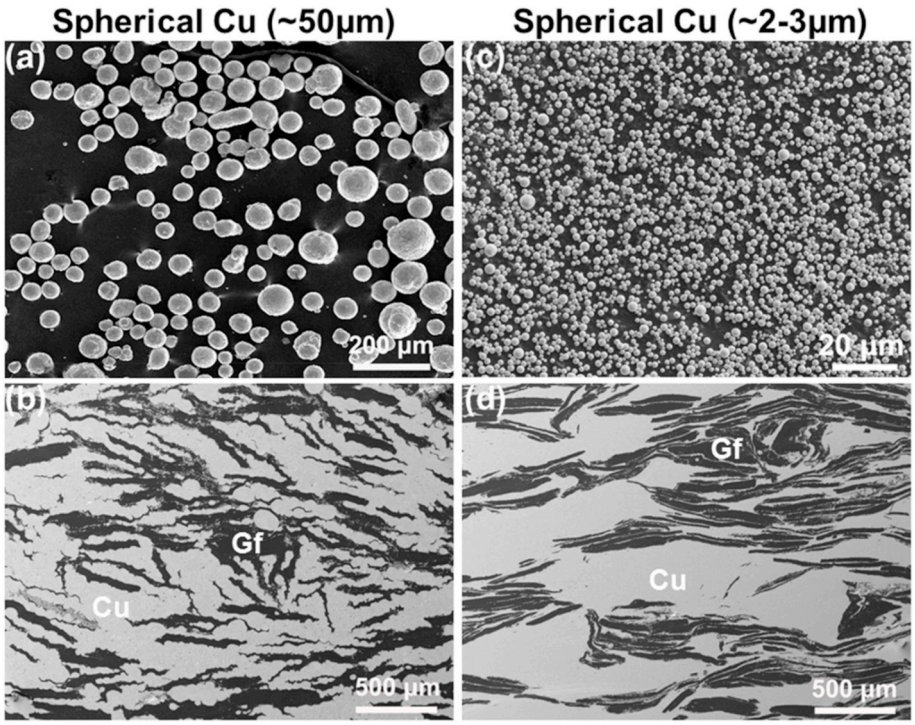

Fig. 3. The pristine morphologies of Cu powders and graphite distributions in 50 vol% Gf/SCu composites. (a–b) The case of spherical Cu powders with a diameter of ~50 μm; (c–d) The case of spherical Cu powders with a diameter of ~2–3 μm.

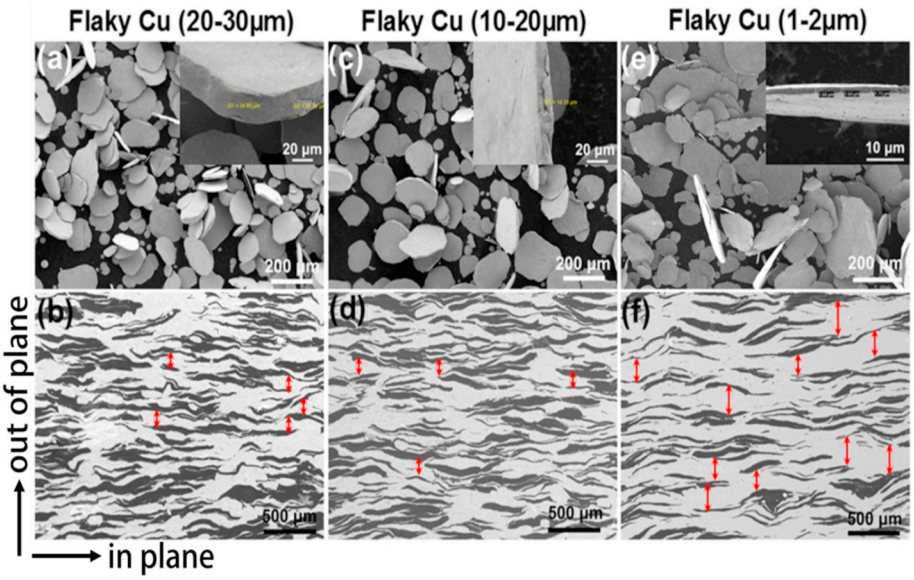

Fig. 4. The pristine morphologies of ball-milled Cu flakes and graphite distributions in 50 vol% Gf/FCu composites along Z axis. The thicknesses of Cu flakes are (a–b) ~20–30 μm, (c–d) ~10–20 μm, and (e–f) ~1–2 μm.

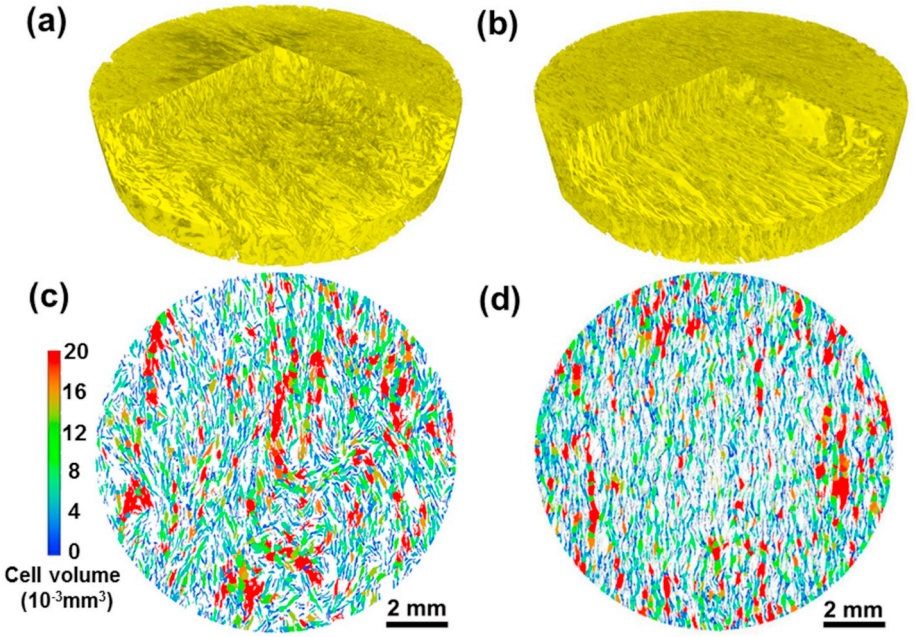

Fig. 5. 2D (different color means different size of the graphite flake) and 3D images (yellow zone is Cu matrix and gray area is graphite in 3D images) for the distribution of graphite flakes in the 50 vol% Gf/Cu composite characterized by 3D X-CT. (a, c) spherical Cu (50 μm) as matrix and (b,d) flaky Cu (1–2 μm) as matrix. (For interpretation of the references to color in this figure legend, the reader is referred to the Web version of this article.)

Information), respectively.

In previous work [13,20], from the polarization-angle dependence of the G peak Raman intensity, the expression was derived for obtaining the graphite flakes alignment by using the selection rules for light scattering in crystals to obtain the intensity of the Raman active modes for an individual graphite flake and then integrating over all possible orientation angles. The overall intensity of graphite flakes in a composite is given by [13,20].

$$I_{tot} \propto \iint \phi(\theta_1,\sigma)\phi(\theta_2,\sigma)I_G(\theta_1,\theta_2)\mathrm{d}_{\theta_1}\mathrm{d}_{\theta_2} + I_0 \tag{2}$$

$$\phi(\theta) = \frac{1}{\sigma\sqrt{2\pi}} e^{-\frac{\theta^2}{2\sigma^2}} \tag{3}$$

where $\phi(\theta,\sigma)$ is the angle distribution for the rotation angles θ_1 and θ_2 and I_0 is a correction term for the Raman setup. Thus, the standard deviation σ remains the parameter for the intensity of the graphite flakes in the copper matrix. Using Eq. (2), σ for different Gf/Cu composites can be obtained. Then from Eq. (1) and Eq. (3), we can obtain the $<\cos^2\theta>$ of the different composites (Table 1).

From Table 1, the $<\cos^2\theta>$ of Gf/FCu composites are much larger than those of Gf/SCu composite. The largest $<\cos^2\theta>$ (0.92) is obtained for the Cu flakes (1–2 μm) as matrix. While the spherical Cu powders as

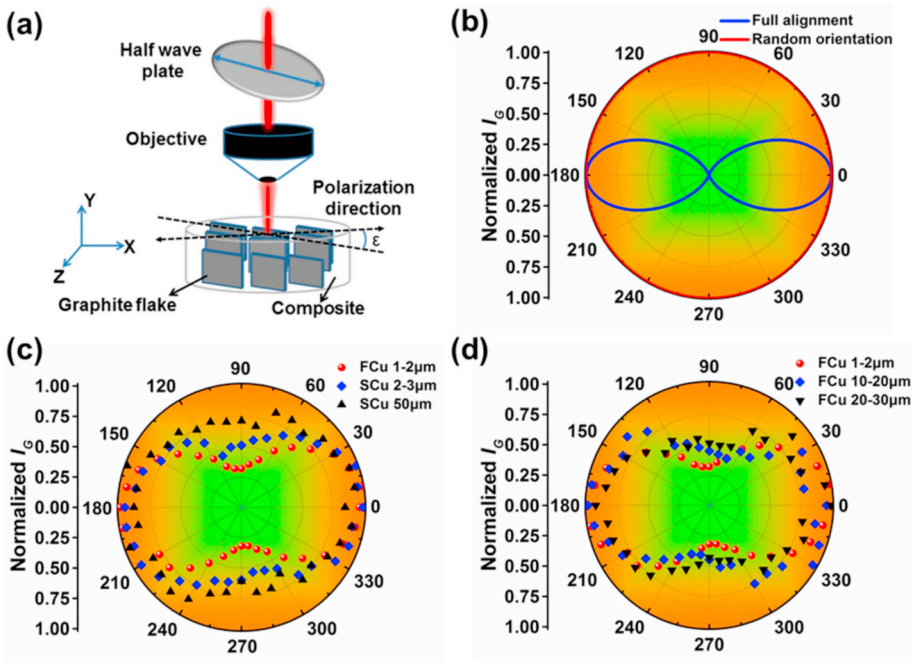

Fig. 6. (a) Measurement setup for polarized Raman spectroscopy; (b) G-mode intensity for randomly oriented and fully aligned graphite flakes; (c–d) Raman intensity of the G peak of graphite as a function of the angle (ε) between the polarization of the light and in-plane direction of 50 vol% Gf/Cu composites: (c) for flaky Cu (1–2 μm), spherical Cu powders (with diameter about 50 μm) and spherical Cu powders (with diameter about 2–3 μm) as matrix; (d) for flaky Cu (1–2 μm, 10–20 μm, and 20–30 μm) as matrix in composites.

Table 1
The parameters for $\langle\cos^2\theta\rangle$ obtained from polarized Raman spectra and $\kappa_{//}$for the different composites.

	Gf/SCu-50 μm	Gf/SCu-2-3 μm	Gf/FCu-20-30 μm	Gf/FCu-10-20 μm	Gf/FCu-1-2 μm
σ	0.55	0.41	0.28	0.26	0.19
$\langle\cos^2\theta\rangle$	0.62	0.74	0.86	0.88	0.92
κ//(W/mK)	372.2 ± 25.1	422.9 ± 28.9	484.6 ± 12.9	510.4 ± 12.2	520.1 ± 9.4

matrix produce low $<\cos^2\theta>$ (0.62 and 0.74). The values of $<\cos^2\theta>$ of different Gf/Cu composites are close to the values obtained from the statistical result of SEM images (Figs. 3 and 4.) as shown in Fig. S5 (Supporting Information). Therefore, the flaky Cu as matrix and hot pressing is able to realize a high alignment degree of graphite in Gf/FCu composite.

3.4. Alignment effect on thermal conductivity

Thermal conductivity of Gf/Cu composites in X–Y plane ($\kappa_{//}$) and Z plane ($\kappa_{\perp}$) direction are shown in Fig. 7a. The composite with flaky Cu (1–2 μm) as matrix exhibits the highest $\kappa_{//}$(520.1 ± 9.4 W/mK) and the lowest $\kappa_{\perp}$ (78.6 ± 1.4 W/mK) among the 50 vol% Gf/Cu composites. 60 vol% Gf/FCu composite shows a high $\kappa_{//}$(570.2 ± 13.9 W/mK) and a low $\kappa_{\perp}$ (66.9 ± 1.7 W/mK). For all the Gf/Cu composites, the $\kappa_{//}$are higher than the $\kappa_{\perp}$ because of anisotropic κ and well orientation of graphite flakes. Fig. 7b shows the anisotropic factor ($\kappa_{//}/\kappa_{\perp}$) of the composites, in which the high alignment degree ($<\cos^2\theta>$) and volume fraction of graphite flakes result in high anisotropic factor. The maximum anisotropic factor (8.52) is obtained at 60 vol% Gf content.

The effective medium approximation (EMA) model is used to predict the theoretical TC of Gf/Cu composite (Fig. S6, Supporting Information). Based on the EMA theory, the anisotropic TC ($\kappa_{\parallel}$, $\kappa_{\perp}$) of the graphite/metal composite can be expressed as [43]:

$$\kappa_{\parallel}=\kappa_m\frac{2+f_g[\beta_{\parallel}(1-L_{\parallel})(1+<\cos^2\theta>)+\beta_{\perp}(1-L_{\perp})(1-<\cos^2\theta>)]}{2-f_g[\beta_{\parallel}L_{\parallel}(1+<\cos^2\theta>)+\beta_{\perp}L_{\perp}(1-<\cos^2\theta>)]} \quad (4)$$

$$\kappa_{\perp}=\kappa_m\frac{1+f_g[\beta_{\parallel}(1-L_{\parallel})(1-<\cos^2\theta>)+\beta_{\perp}(1-L_{\perp})<\cos^2\theta>]}{1-f_g[\beta_{\parallel}L_{\parallel}(1-<\cos^2\theta>)+\beta_{\perp}L_{\perp}<\cos^2\theta>]} \quad (5)$$

where κ_m is the TC of the matrix, f_g is the volume fraction of graphite, β and L are the factors related to the geometry of graphite and interfacial thermal resistance (R_k) (detailed deduction is shown in Supporting Information). In these calculations, the TC of the graphite flakes is set as follows: $\kappa_{g//}$= 1020 W/mK, which is in agreement to the estimation from $d_{(002)}$ by Adams' study [42]. The value of κ_m is 380 W/mK and R_k is assumed as 1.0×10^{-9} m^2K/W. The $\kappa_{\parallel}$ and $\kappa_{\perp}$ dependences on $<\cos^2\theta>$ based on EMA model are shown in Fig. 7c–d. The results show that $<\cos^2\theta>$ is a crucial factor for $\kappa_{//}$and $\kappa_{\perp}$, and an increased $\kappa_{//}$can be attained by increasing $<\cos^2\theta>$ at the same content of graphite. From Fig. 7c, under such R_K (10^{-9} m^2/kW), the numerical results demonstrate that the aligned graphite flakes cannot lead to $\kappa_{//}$enhancement if $<\cos^2\theta>$ < 0.62, which elucidates that the $\kappa_{//}$enhancement induced by the aligned graphite is largely suppressed by the adverse effect of R_K. Hence, to obtain the increased $\kappa_{//}$, one needs to achieve the alignment degree at $<\cos^2\theta>$ > 0.62 and reduce the R_K. Boden et al. [20] observed no obviously enhanced effect of graphite on the $\kappa_{//}$of 30 vol% Gf/Cu composites though the $<\cos^2\theta>$ was 0.69. The main reason is that 0.69 was still below a critical $<\cos^2\theta>$ in the prepared Gf/Cu composites. Moreover, an extraordinary $\kappa_{//}$of 640 W/mK can be expected for the 60 vol% Gf/Cu composites with nearly perfect graphite alignment at $<\cos^2\theta>$ of 0.92 (Fig. 7c). Note that the same $\kappa_{//}$can also be obtained by largely increasing f_g over 80 vol% at a low $<\cos^2\theta>$. Thus, to economically gain a desired $\kappa_{//}$, optimizing $<\cos^2\theta>$ may offer a practical way to realize the remarkable graphite saving. In Fig. 7d, $\kappa_{\perp}$ shows a decreased tendency with the increase of graphite content. Higher alignment degree ($<\cos^2\theta>$) of graphite leads to lower $\kappa_{\perp}$ due to the low $\kappa_{\perp}$ of graphite in this direction. In Fig. 7e, based on EMA calculations, the results show that an increased anisotropic factor can be attained by increasing graphite content or/and increasing $<\cos^2\theta>$.

The anisotropic effect of the thermal properties of 60 vol% Gf/FCu composite were also characterized by an infrared (IR) camera. Fig. 8a, c shows the schematics of the Gf/FCu composites (parallel and perpendicular to the graphite alignment direction, respectively), with the bottom surfaces being placed on a hot plate (not shown). The hot plate acted as a heat source providing continuous and stable power input to

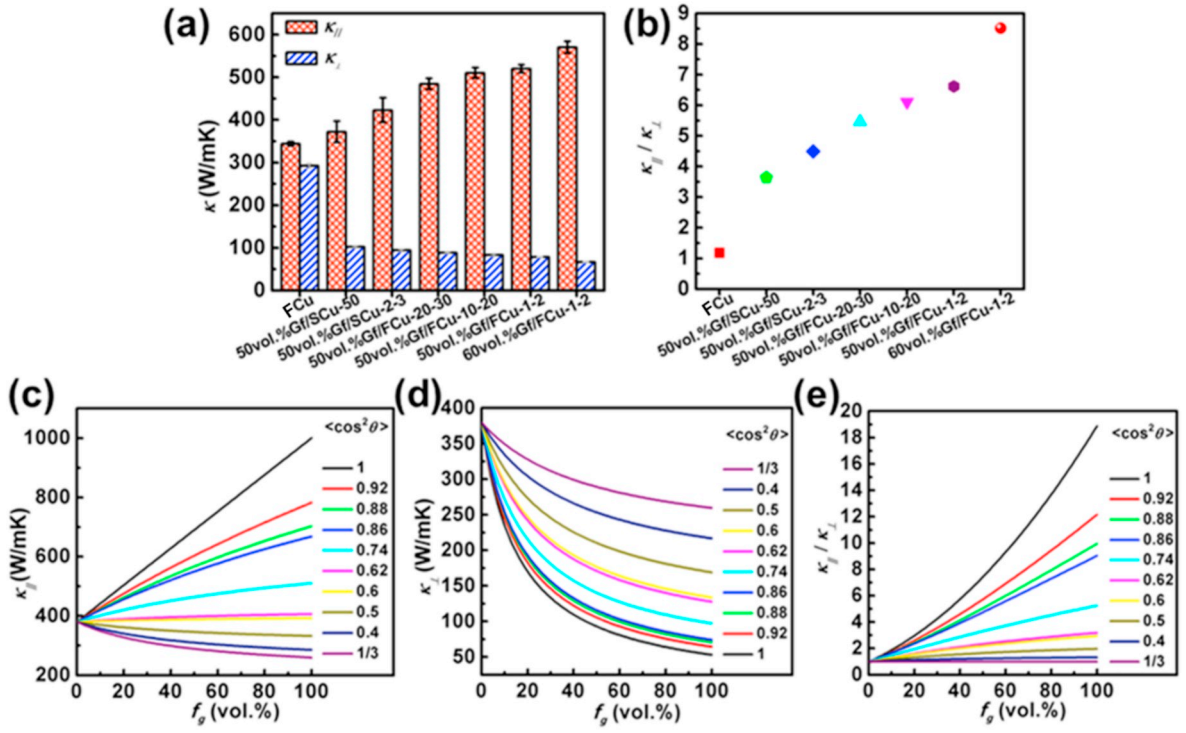

Fig. 7. Anisotropic thermal conductivity of Gf/FCu composites. (a) Thermal conductivity of the different Gf/Cu composites in the X–Y plane direction ($\kappa_{//}$) and Z plane direction ($\kappa_{\perp}$); (b) Anisotropic factor ($\kappa_{//}/\kappa_{\perp}$) of thermal conductivity for the different composites; (c–d) EMA numerical results of $\kappa_{//}$(c) and $\kappa_{\perp}$ (d) versus f_g at different $<\cos^2\theta>$ for the Gf/Cu composites; (e) Anisotropic factor ($\kappa_{//}/\kappa_{\perp}$) of the numerical results based on EMA.

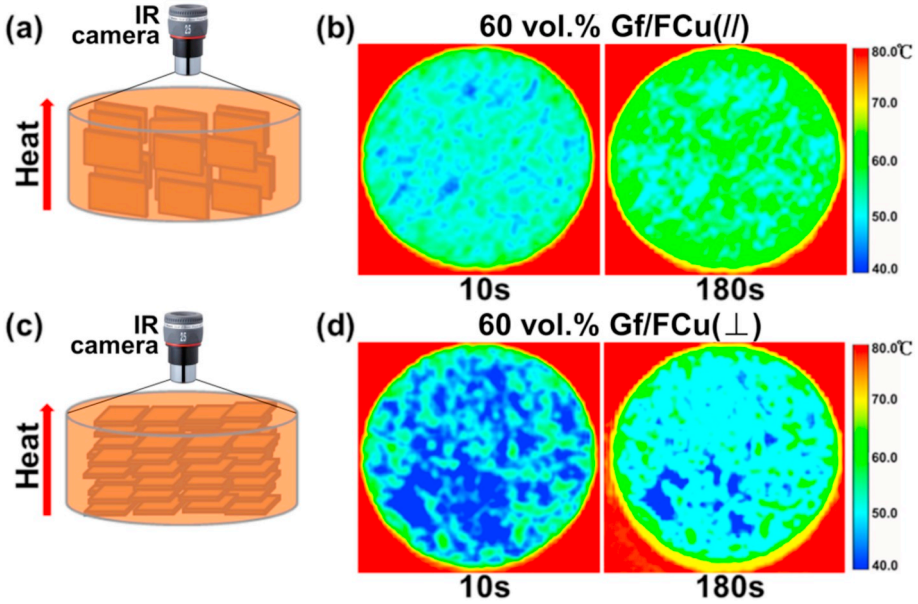

Fig. 8. Demonstration of highly anisotropic thermal properties of 60 vol% Gf/FCu composite. All the diameters of the samples and observed areas are 12.6 mm. (a) Heat-transfer schematic and (b) IR thermographic images of the composite with the incident heat parallel to the graphite alignment direction; (c) Heat-transfer schematic and (d) IR thermographic images of the composite with the incident heat perpendicular to the graphite alignment direction.

the bottom surface of the composite. Temperature of the hot plate was set at 80 °C. The resulting changes in temperature distribution profile of the top surface for the sample was monitored and recorded by an IR camera. Fig. 8b shows the surface temperature contour of the composite (parallel to graphite alignment) at various times. Since the graphite alignment direction is parallel to the direction of heat flow, the heat transfers more effectively in this direction. As a result, at 180 s, a steady state temperature distribution in the composite was reached, with a maximum temperature of 60 °C on the top surface of the composite (the difference from 80 °C of the hot plate is due to heat loss). In another direction, the temperature contour shows insufficient heat transfer to the top surface (Fig. 8d). The steady state maximum temperature on the top surface was reached at 180s with a value of 54 °C. Thermographic figures clearly demonstrate that the composite along the graphite

alignment direction shows a higher TC. As shown in Fig. 8a–b, this high alignment of graphite makes it possible for Gf/FCu composite to be integrated in thermal dissipation applications. High surface temperature is a result of the effective heat dissipation to the upper side of the sample in this direction. In another direction, the heat transfer path is blocked due to the low TC between the separated Cu matrix channels and low $\kappa_{\perp}$ of graphite flakes (Fig. 8c–d), reducing heat radiation to the surrounding electronic components in thermal management application.

3.5. Interface modification and characterization of Gf/Gr/FCu composites

Apart from alignment of graphite in Gf/Cu composite, interfacial bonding between graphite and Cu also shows a significant effect on the thermal conductivity. In Gf/FCu composite, the observed interface is discontinuous and obvious gaps between graphite and Cu exist (Fig. 9a). These voids were generated during cooling process after sintering due to the different extent of shrinkage and poor interfacial bonding in the composite [44]. Beyond the two main conventional methods (i.e. surface metallization and matrix alloying), here, graphene (Gr) in situ grown on the Cu flakes is used to improve the interface compatibility. SEM images of the surface morphology of in situ grown Gr/FCu powders (Fig. 9b–c) show that relatively thin graphene film with some wrinkles is found on the copper surface. From our previous work [41], the content of graphene is estimated at 0.35 vol% in the composite. D, G band in Raman spectra of Gr/Cu powders confirm the structure of in situ grown graphene with some defects (Fig. 9d). SEM image of typical interface microstructure of Gf/Gr/FCu composites in Fig. 9e shows that a distinctly close contact and continuous interface without obvious gaps between Cu and graphite are observed with interfacial modification by the graphene. Elemental line distribution results across interface shows a discontinuous distribution of C element across the interface in Gf/FCu composite due to existence of voids, while Gf/Gr/FCu composites presents a continuous elemental distribution (Fig. S7, Supporting Information). The SEM images demonstrate a highly oriented and uniformly arranged graphite in the matrix (Fig. S8 Supporting Information) after modification by graphene. To evaluate the interfaces between Cu matrix and graphite in more detail, TEM was used to examine the microstructures of the Gf/FCu and Gf/Gr/FCu composites. In Gf/FCu composites, some voids exist at Gf-Cu interface (Fig. S9a, Supporting Information). In Gf/Gr/FCu composite, there are three distinct areas: Cu matrix, interlayer region and graphite (Fig. S9b, Supporting Information). EDS result indicates this area contains Cu and C elements (Fig. S10, Supporting Information). HR-TEM image of the Gf/Gr/FCu interface (Fig. 9f) reveals that there is a representative graphene interlayer. For the graphene-copper interface, because the graphene layers were directly grown on the copper surface by in situ catalytic process, pore formation was suppressed at the graphene-Cu interface. This is different from the external addition method, and it is also an advantage over the external addition of graphene nanoplates or graphene oxide in Cu matrix. The schematic illustrations of the interface structures of Gf/Cu and Gf/Gr/Cu composites are shown in Fig. S11 (Supporting Information). Interface modification by surface metallization or matrix alloying may lead to complex composition of the interlayers, eg. TiC + Ti. The multiphase is adverse to the interfacial thermal conductance. Differing from surface metallization and matrix alloying, the in situ grown graphene interlayer with nanometer thickness and high TC for interfacial modification has only a stable single phase and avoid direct contact between graphite and Cu, which is beneficial to improvement of TC for Gf/Gr/FCu composites.

3.6. Thermal properties of bulk Gf/Gr/FCu composites

From Fig. 7a, the composite with flaky Cu (1–2 μm) as matrix exhibits the highest TC. So the flaky Cu (1–2 μm) was used as matrix for in situ growth of graphene. Fig. 10 shows the experimental TCs of the obtained Gf/Gr/FCu composites in two directions after interfacial modification by graphene, as well as TCs of Gr/FCu composites and FCu pure matrix prepared by the same method. The detailed parameters of TC calculation are shown in Table S1 (Supporting Information). From Fig. 10a, it is visibly seen that the $\kappa_{//}$of Gf/Gr/FCu composites are higher than those of Gf/FCu counterparts (Fig. 7a). The $\kappa_{//}$of 50 vol% and 60 vol% Gf/FCu increase from 520.1 ± 9.4 to 552.6 ± 11.8 W/mK and from 570.2 ± 13.9 to 597.1 ± 20.9 W/mK with incorporation of graphene, respectively. Additionally, the composite shows a low density which is 40% lighter than that of Cu counterpart. The improvement can be ascribed to the following reason. The existed micro-voids and air gaps between graphite and Cu matrix can induce strong phonon scattering, which is detrimental to the heat transfer. After interfacial modification, the graphene interlayer exhibiting a high TC will replace the voids,

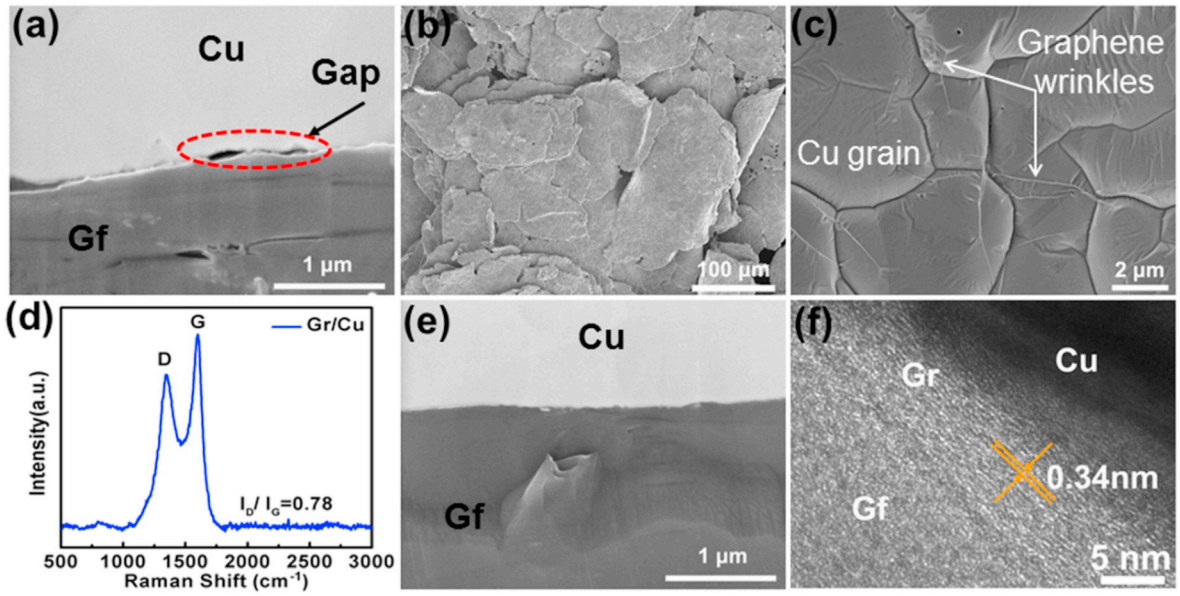

Fig. 9. (a) SEM images of Gf-Cu interface; (b–c) SEM images of in situ grown graphene/Cu (flaky Cu, 1–2 μm) composited powders; (d) Raman spectra of in situ grown Gr/FCu powders; (e) SEM image and (f) HR-TEM image for the interface microstructure in Gf/Gr/FCu composite.

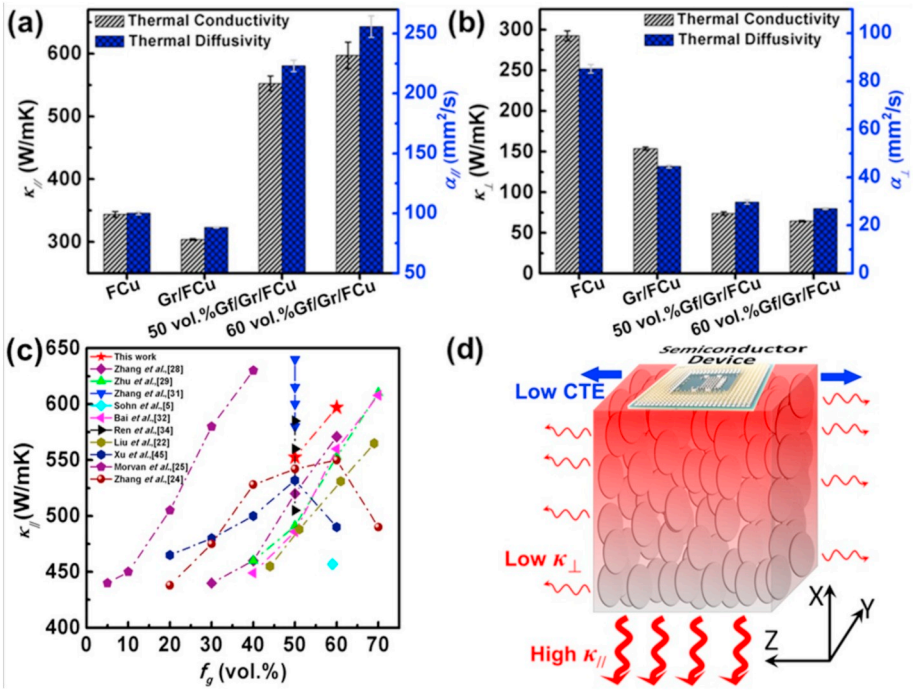

Fig. 10. (a–b) Thermal conductivity (κ) and thermal diffusivity (α) of Cu, Gr/FCu, Gf/Gr/FCu composites: (a) in X–Y direction ($\kappa_{//}$, $\alpha_{//}$); (b) in z-direction ($\kappa_{\perp}$, $\alpha_{\perp}$); (c) comparison of thermal conductivity of Gf/Gr/FCu composites with the thermal conductivities for reported Gf/Cu composites in literatures [5,22,24,25,28,29,31,32,34,45]; (d) Schematic illustration of the Gf/Gr/FCu composite with high $\kappa_{//}$and low CTE connected to a semiconductor device for heat dissipation.

reducing phonon scattering and improving interfacial thermal conductivity. The increment of TC is about 30 W/mK, which is much lower over diamond/Cu composite due to high increment (~4%) of relative density in Dia/Cu composite [40]. On one hand, interfacial modification does not provide an obviously enhancing effect on the relative density. Though some voids still exist in the Gf/FCu composites without modification, the high relative density are close to 99%, resulting in high TC. On the other hand, at a high alignment degree ($<\cos^2\theta> > 0.9$) of graphite within Cu matrix, the decreased interfacial thermal resistance would only result in a low increment (30–50 W/mK) because the TC is dominated by the alignment of graphite instead of interfacial thermal resistance [12,20]. At a low alignment degree, a large increment of TC can be achieved by lowering the interfacial thermal resistance [12]. Interfacial modification by 0.35 vol% graphene still provides a positive effect on the TC. While too thick graphene layers will lead to high interfacial thermal resistance [40] and reduce the TC of Gf/Gr/FCu composites. The $\kappa_{//}$of 60 vol% Gf/Gr/FCu is close to the theoretical value (640 W/mK, from Fig. 7c) due to the improved interfacial bonding. The discrepancy between experimental value and theoretical value are likely due to the following factors. On one hand, the poorly crystalline graphite zone at the graphene/Gf interface aggravate phonon scattering, giving rise to deterioration of heat transport ability [31]. On the other hand, the residual graphene layers in the Cu matrix will generate phonon scattering and more or less decrease the TC, as reported in our previous work [41]. Fig. 10b shows $\kappa_{\perp}$ of the Gf/Gr/FCu composites. The TCs of the composites are only slightly decreased when graphene was introduced on Cu surface.

As compared in Figs. 10c and 597.1 W/mK of the 60 vol% Gf/Gr/FCu composites is relatively prominent among the TCs for reported Gf/Cu composites with interfacial modification by surface metallization or matrix alloying as well as pre-treatment of graphite [5,22,24,25,28,29,31,32,34,45]. Morvan et al. [25] used reductive thermal pre-treated graphite as reinforcement to obtain high TC of Gf/Cu composite by optimizing powder processing methodology (PPM). Zhang et al. [31] and Ren et al. [34] optimized the content of Zr and Cr to achieve high TC of Gf/Cu composites, respectively. With 50–60 vol% graphite, the obtained TC is comparable to the reported data.

In practical application, CTE is an important property for thermal management materials. Fig. S12 (Supporting Information) show that composites with 50 vol% and 60 vol% graphite in X–Y plane direction display similar variation trends of relative length and corresponding CTEs. In Z plane direction, the CTE of 60 vol% Gf/Gr/FCu composite is 6 ppm/K because of high alignment graphite and the improved interfacial bonding. Along X–Y plane direction, the high $\kappa_{//}$of the composite provides effectively heat dissipation channels when connected to semiconductor devices (Fig. 10d). In Z plane direction, the low $\kappa_{\perp}$ can reduce heat radiation to surrounding electronic components, while CTE matched with semiconductors can protect the devices from thermal failure. Thus, the high $\kappa_{//}$and low CTE make Gf/Gr/FCu composites be a promising heat sink materials in thermal management.

4. Conclusions

To obtain high thermal conductivity and low coefficient of thermal expansion, graphite/graphene/Cu composites with high alignment of graphite and improved interfacial bonding were achieved by controlling morphologies and size of copper powders and using in situ grown graphene as interlayer. The main conclusions are summarized as follows.

(1) High alignment of graphite in Gf/Cu composite was obtained by controlling the morphology and size of Cu matrix particle. As quantified by polarized Raman spectra, the flaky Cu with a thickness of 1–2 μm contributed to a high orientation degree ($<\cos^2\theta> = 0.92$) of graphite flakes in Cu matrix, leading to a high anisotropic factor ($\kappa_{//}/\kappa_{\perp}$). The maximum of anisotropic factor was 8.52 for 60 vol% Gf/FCu composite. The strategy is also available for regulating alignment of other two-dimensional micro-/nanoplates (Such as boron nitride (BN) [46] and MXene phases [47,48] etc.) in a composite matrix and thus tailoring the thermal properties.

(2) Differing from surface metallization and matrix alloying for interfacial modification, in situ grown graphene on Cu surface

was utilized as interlayer for interfacial modification. The TC of 50 vol% Gf/Gr/FCu increased to 552.6 W/mK 60 vol% graphite content exhibited a TC of 597.1 W/mK. CTE of the 60 vol% Gf/Gr/FCu composites in Z direction decreased to 6 ppm/K. Additionally, the composite is 40% lighter than Cu.

(3) Hot pressing treatment under Argon atmosphere at 1173 K improved crystallinity structure of graphite flakes as confirmed by XRD and Raman spectroscopy measurements. The TC of graphite increased from 500 W/mK to 1020 W/mK after hot pressing. This enhancement provides new insight in analysis thermal conductivity of graphite/metal matrix composites, and also a simple method to improve thermal conductivity of graphite filler.

Declaration of competing interest

The authors declare that they have no known competing financial interests or personal relationships that could have appeared to influence the work reported in this paper.

CRediT authorship contribution statement

Huaijie Cao: Investigation, Writing - original draft. **Zhanqiu Tan:** Data curation, Resources. **Genlian Fan:** Visualization, Investigation. **Qiang Guo:** Writing - review & editing. **Yishi Su:** Software. **Zhiqiang Li:** Writing - review & editing. **Ding-Bang Xiong:** Supervision, Project administration, Funding acquisition, Writing - review & editing.

Acknowledgments

This work was supported by the National Key R&D Program of China (No.2017YFB0406200), the National Natural Science Foundation of China (Nos. 51771110, 51971131, 51371115, 51671130, 51771111), the Shanghai Science & Technology Committee (Nos. 15JC1402100, 17520712400), the Ministry of Science & Technology of China (No. 2016YFE0130200).

Appendix A. Supplementary data

Supplementary data to this article can be found online at https://doi.org/10.1016/j.compositesb.2020.107965.

References

[1] Moore AL, Shi L. Emerging challenges and materials for thermal management of electronics. Mater Today 2014;17:163–74.
[2] Song HF, Liu JM, Liu BL, Wu JQ, Cheng HM, Kang FY. Two-dimensional materials for thermal management applications. Joule 2018;2:442–63.
[3] Kang JS, Li M, Wu HA, Nguyen H, Hu YJ. Experimental observation of high thermal conductivity in boron arsenide. Science 2018;361:575–8.
[4] Cui QY, Yu CW, Hao JJ, Chen CG, Zhang XD, Guo ZM, Volinsky AA. Ultrahigh thermal conductivity copper/graphite membrane composites prepared by tape casting with hot-pressing sintering. Mater Lett 2018;231:60–3.
[5] Sohn Y, Han T, Han JH. Effects of shape and alignment of reinforcing graphite phases on the thermal conductivity and the coefficient of thermal expansion of graphite/copper composites. Carbon 2019;149:152–64.
[6] Chen JK, Huang IS. Thermal properties of aluminum-graphite composites by powder metallurgy. Compos B Eng 2013;44. 698-3.
[7] Nazeer F, Ma Z, Gao LH, Wang FC, Khan MA, Malik A. Thermal and mechanical properties of copper-graphite and copper-reduced graphene oxide composites. Compos B Eng 2019;163:77–85.
[8] Pop E, Varshney V, Roy AK. Thermal properties of graphene: fundamentals and applications. MRS Bull 2012;37:1273–81.
[9] Balandin AA. Thermal properties of graphene and nanostructured carbon materials. Nat Mater 2011;10:569–81.
[10] Khaleghi E, Torikachvili M, Meyers MA, Olevsky EA. Magnetic enhancement of thermal conductivity in copper-carbon nanotube composites produced by electroless plating, freeze drying, and spark plasma sintering. Mater Lett 2012;79:256–8.
[11] Wejrzanowski T, Grybczuk M, Chmielewski M, Pietrzak K, Kurzydlowski KJ, Strojny-Nedza A. Thermal conductivity of metal-graphene composites. Mater Des 2016;99:163–73.
[12] Chu K, Wang XH, Wang F, Li YB, Huang DJ, Liu H, Ma WL, Liu FX, Zhang H. Largely enhanced thermal conductivity of graphene/copper composites with highly aligned graphene network. Carbon 2018;127:102–12.
[13] Firkowska I, Boden A, Boerner B, Reich S. The origin of high thermal conductivity and ultralow thermal expansion in copper-graphite composites. Nano Lett 2015;15:4745–51.
[14] Jang J-H, Park H-K, Lee J-H, Lim J-W, Oh I-H. Effect of volume fraction and unidirectional orientation controlled graphite on thermal properties of graphite/copper composites. Compos B Eng 2020;183:107735.
[15] Fu Q, Yang JK, Chen YF, Li DY, Xu DY. Experimental evidence of very long intrinsic phonon mean free path along the c-axis of graphite. Appl Phys Lett 2015;106:031905.
[16] Taylor R. The thermal conductivity of pyrolytic graphite. Philos Mag 1966;13:157–66.
[17] Shuai J, Xiong LQ, Zhu L, Li WZ. Enhanced strength and excellent transport properties of a superaligned carbon nanotubes reinforced copper matrix laminar composite. Compos Part A Appl Sci Manuf 2016;88:148–55.
[18] Chu K, Wang XH, Li YB, Huang DJ, Geng ZR, Zhao XL, Liu H, Zhang H. Thermal properties of graphene/metal composites with aligned graphene. Mater Des 2018;140:85–94.
[19] Nazeer F, Ma Z, Xie YT, Gao LH, Malik A, Khan MA, Wang FC, Li HZ. A novel fabrication method of copper-reduced graphene oxide composites with highly aligned reduced graphene oxide and highly anisotropic thermal conductivity. RSC Adv 2019;9:17967–74.
[20] Boden A, Boerner B, Kusch P, Firkowska I, Reich S. Nanoplatelet size to control the alignment and thermal conductivity in copper-graphite composites. Nano Lett 2014;14:3640–4.
[21] Wu S, Li TX, Tong Z, Chao JW, Zhai TY, Xu JX, Yan TS, Wu MQ, Xu ZY, Bao H, Deng T, Wang RZ. High-performance thermally conductive phase change composites by large-size oriented graphite sheets for scalable thermal energy harvesting. Adv Mater 2019:1905099.
[22] Liu Q, He XB, Ren SB, Zhang C, Liu TT, Qu XH. Thermophysical properties and microstructure of graphite flake/copper composites processed by electroless copper coating. J Alloys Compd 2014;587:255–9.
[23] Liu B, Zhang DQ, Li XF, He Z, Guo XH, Liu ZJ, Guo QG. Effect of graphite flakes particle sizes on the microstructure and properties of graphite flakes/copper composites. J Alloys Compd 2018;766:382–90.
[24] Zhang C, He XB, Liu Q, Ren SB, Qu XH. Fabrication and thermo-physical properties of graphite flake/copper composites. J Compos Mater 2015;49:3323–30.
[25] Morvan A, Grosseau-Poussard JL, Caillault N, Delange F, Roure S, Lepretre P, Silvain J-F. Powder processing methodology for fabrication of Copper/Graphite composite materials with enhanced thermal properties. Compos Part A Appl Sci Manuf 2019;124:105474–82.
[26] Delannay F, Froyen L, Deruyttere A. The wetting of solids by molten metals and its relation to the preparation of metal-matrix composites composites. J Mater Sci 1987;22:1–16.
[27] Lloyd JC, Neubauer E, Barcena J, Clegg WJ. Effect of titanium on copper-titanium/carbon nanofibre composite materials. Compos Sci Technol 2010;70:2284–9.
[28] Zhang R, He X, Liu Q, Qu XH. Improvement in mechanical and thermal properties of graphite flake/Cu composites by introducing TiC coating on graphite flake surface. Metals 2019;9:519.
[29] Zhu YB, Bai H, Xue C, Zhou R, Xu QF, Tao P, Wang C, Wang JW, Jiang N. Thermal conductivity and mechanical properties of a flake graphite/Cu composite with a silicon nano-layer on a graphite surface. RSC Adv 2016;6:98190–6.
[30] Liu Q, He XB, Ren SB, Liu TT, Kang QP, Qu XH. Fabrication and thermal conductivity of copper matrix composites reinforced with Mo2C or TiC coated graphite fibers. Mater Res Bull 2013;48:4811–7.
[31] Zhang R, He XB, Chen HT, Qu XH. Effect of alloying element Zr on the microstructure and properties of graphite flake/Cu composites fabricated by vacuum hot pressing. J Alloys Compd 2019;770:267–75.
[32] Bai H, Xue C, Lyu JL, Li J, Chen GX, Yu JH, Lin CT, Lv DJ, Xiong LM. Thermal conductivity and mechanical properties of flake graphite/copper composite with a boron carbide-boron nano-layer on graphite surface. Compos Part A Appl Sci Manuf 2018;106:42–51.
[33] Yang WL, Zhou LP, Peng K, Zhu JJ, Wan L. Effect of tungsten addition on thermal conductivity of graphite/copper composites. Compos B Eng 2013;55:1–4.
[34] Ren SB, Chen JH, He XB, Qu XH. Effect of matrix-alloying-element chromium on the microstructure and properties of graphite flakes/copper composites fabricated by hot pressing sintering. Carbon 2018;127:412–23.
[35] Zhang R, He XB, Chen Z, Qu XH. Influence of Ti content on the microstructure and properties of graphite flake/Cu-Ti composites fabricated by vacuum hot pressing. Vacuum 2017;141:265–71.
[36] Yuan MY, Tan ZQ, Fan GL, Xiong D-B, Guo Q, Guo CP, Li ZQ, Zhang D. Theoretical modelling for interface design and thermal conductivity prediction in diamond/Cu composites. Diam Relat Mater 2018;81:38–44.
[37] Chang G, Sun FY, Wang LH, Che ZX, Wang XT, Wang JG, Kim MJ, Zhang HL. Regulated interfacial thermal conductance between Cu and diamond by a TiC interlayer for thermal management applications. ACS Appl Mater Interfaces 2019;11:26507–17.
[38] Chang G, Sun FY, Duan JL, Che ZF, Wang XT, Wang JG, Kim MJ, Zhang HL. Effect of Ti interlayer on interfacial thermal conductance between Cu and diamond. Acta Mater 2018;160:235–46.
[39] Balandin AA, Ghosh S, Bao WZ, Calizo I, Teweldebrhan D, Miao F, Lau CN. Superior thermal conductivity of single-layer graphene. Nano Lett 2008;8:902–7.
[40] Cao HJ, Tan ZQ, Lu MH, Ji G, Yan XJ, Di C, Yuan MY, Guo Q, Su YS, Addad A, Li ZQ, Xiong D-B. Graphene interlayer for enhanced interface thermal conductance

in metal matrix composites: an approach beyond surface metallization and matrix alloying. Carbon 2019;150:60–8.
[41] Cao HJ, Xiong D-B, Tan ZQ, Fan GL, Li ZQ, Guo Q, Su YS, Guo CP, Zhang D. Thermal properties of in situ grown graphene reinforced copper matrix laminated composites. J Alloys Compd 2019;771:228–37.
[42] Adams PM, Katzman HA, Rellick GS, Stupian GW. Characterization of high thermal conductivity carbon fibers and a self-reinforced graphite panel. Carbon 1998;36:233–45.
[43] Nan C-W, Birringer R, Clarke DR, Gleiter H. Effective thermal conductivity of particulate composites with interfacial thermal resistance. J Appl Phys 1997;81:6692–9.
[44] Chen JH, Ren SB, He XB, Qu XH. Properties and microstructure of nickel-coated graphite flakes/copper composites fabricated by spark plasma sintering. Carbon 2017;121:25–34.
[45] Xu H, Chen JH, Ren SB, He XB, Qu XH. Sintering behavior and thermal conductivity of nickel-coated graphite flake/copper composites fabricated by spark plasma sintering. Int J Min Met Mater 2018;25:459–71.
[46] Wang HT, Ding DL, Liu Q, Chen YH, Zhang QY. Highly anisotropic thermally conductive polyimide composites via the alignment of boron nitride platelets. Compos B Eng 2019;158:311–8.
[47] Zhang Q, Yi G, Fu Z, Yu H, Chen S, Quan X. Vertically aligned janus MXene-based aerogels for solar desalination with high efficiency and salt resistance. ACS Nano 2019;13:13196–7.
[48] Liu ZJ, Yin CG, Cecen V, Fan JC, Shi PH, Xu QJ, et al. Polybenzimidazole thermal management composites containing functionalized boron nitride nanosheets and 2D transition metal carbide MXenes. Polymer 2019;179:12613–22.